Applied Mathematics Letters 148 (2024) 108880

Contents lists available at ScienceDirect

Applied Mathematics Letters

www.elsevier.com/locate/aml

Efficient low-rank quaternion matrix completion under the learnable transforms for color image recovery

Pengling Wu [a], Kit Ian Kou [a,*], Jifei Miao [b]

[a] Department of Mathematics, Faculty of Science and Technology, University of Macau, 999078, Macao Special Administrative Region of China
[b] The School of Mathematics and Statistics, Yunnan University, Kunming, Yunnan, 650091, China

A R T I C L E I N F O

Article history:
Received 18 August 2023
Received in revised form 27 September 2023
Accepted 27 September 2023
Available online 29 September 2023

Keywords:
Low-rank quaternion matrix completion
Semi-orthogonal transform
Weighted Schatten p-norm
Color image recovery
Alternating direction method of multipliers

A B S T R A C T

Recent low-rank quaternion matrix completion (LRQMC) approaches have been extensively studied to recover missing data of color images. However, these methods need to frequently compute the quaternion singular value decompositions (QSVD) of the quaternion matrix, making them unsuitable for large-scale data. In this paper, we suggest an efficient LRQMC model based on the learnable transforms for color image recovery. The key idea is to project the large-scale quaternion matrix to a small-scale quaternion matrix via the semi-orthogonal transforms along each mode, which significantly reduces the computational cost of QSVD. We then apply a nonconvex approximation of rank (i.e., weighted Schatten p-norm) onto the small-scale quaternion matrix to achieve a better quaternion rank estimation. The alternating direction method of multipliers scheme is developed to solve the proposed model, and the weak convergence property of the algorithm is discussed. Experimental results on color images demonstrate that our method is considerably faster than state-of-art approaches while achieving comparative recovery performance.

1. Introduction

Color image recovery, which recovers missing values from the observed image, is a fundamental problem in color image processing [1,2]. The color image consists of three highly correlated channels, which enriches faithful representation of real scenes. Unfortunately, color images in different areas are often incomplete due to limitations in acquisition and transmission. Hence, recovering missing data is of great importance for real-world applications.

Recently, the quaternion has emerged as an elegant mathematical tool in color image processing, primarily due to its capability of well preserving the color structure of images [3,4]. A quaternion comprises one real part and three imaginary components [5], leading to a natural way to represent and process color images.

* Corresponding author.
E-mail addresses: wupengling@163.com (P. Wu), kikou@umac.mo (K.I. Kou), jifmiao@163.com (J. Miao).

https://doi.org/10.1016/j.aml.2023.108880
0893-9659/

Using quaternion representation (QR), a color image with the size of $I_1 \times I_2 \times 3$ can be encoded as a pure quaternion matrix $\dot{\mathbf{X}}$ with the red, green and blue channel pixel values on the three imaginary components, respectively, i.e., $\dot{\mathbf{X}}_{ij} = \mathbf{R}_{ij}\mathbf{i} + \mathbf{G}_{ij}\mathbf{j} + \mathbf{B}_{ij}\mathbf{k}, 1 \leq i \leq I_1, 1 \leq j \leq I_2$, where $\mathbf{R}_{ij}, \mathbf{G}_{ij}$, and $\mathbf{B}_{ij}$ are the red, green, and blue pixel values, respectively, and $\mathbf{i}, \mathbf{j}, \mathbf{k}$ are the three imaginary units of a quaternion. This means that all color channels are processed holistically in the quaternion domain [6,7], which can well integrate the information of three channels and capture the correlation among three channels. Utilizing the benefits of QR, numerous QR-based works have emerged, yielding promising results in color image tasks, such as color image inpainting [8,9], color image classification [10,11], and color face recognition [12,13].

Quaternion matrix completion is a common approach for recovering missing data in color images. It aims to recover the underlying quaternion matrix from its incomplete observations under the low-rank assumption, and its mathematical model is formulated as

$$\min_{\dot{\mathbf{X}}} \ \mathrm{rank}(\dot{\mathbf{X}}), \quad \text{s.t.} \ \ P_{\Omega}(\dot{\mathbf{X}}) = P_{\Omega}(\dot{\mathbf{Y}}), \tag{1}$$

where $\mathrm{rank}(\cdot)$ denotes the rank function, $\dot{\mathbf{X}} \in \mathbb{Q}^{I_1 \times I_2}$ and $\dot{\mathbf{Y}} \in \mathbb{Q}^{I_1 \times I_2}$ represent the recovered and observed quaternion matrices, respectively, Ω is the observed elements set, and $P_{\Omega}(\dot{\mathbf{X}})$ is a projection operator where $P_{\Omega}(\dot{\mathbf{X}})_{ij} = \dot{\mathbf{X}}_{ij}$ if $(i,j) \in \Omega$ and 0 otherwise. Recently, Chen *et al*. [14] proposed a general low-rank quaternion matrix approximation (LRQA) model based on the quaternion nuclear norm (QNN) and several nonconvex functions. However, the computation of quaternion singular value decomposition (QSVD) [5] in each iteration step results in high time consumption. To reduce the time consumption, Miao *et al*. [15] suggested three low-rank quaternion matrix completion (LRQMC) models that only require handling two smaller factor quaternion matrices via the quaternion bilinear factorization. Yang *et al*. [16] introduced the truncated nuclear norm-based QMC method for color image recovery. Furthermore, Yang *et al*. [17] introduced the nonconvex quaternion matrix logarithmic norm to achieve a more precise approximation of the rank. While the complexity of nonconvex functions also results in high computational cost, especially when dealing with large-scale data.

In this paper, we propose the learnable transforms-based nonconvex LRQMC model (TN-LRQMC) for color image recovery, which can achieve substantial speedup while maintaining accuracy compared to state-of-the-art approaches. To begin, we project the large-scale quaternion matrix into a small-scale quaternion matrix with the learnable semi-orthogonal transforms along each mode. Subsequently, we introduce the weighted Schatten p-norm as a nonconvex approximation of rank to better explore the low-rank structure of the small-scale quaternion matrix. In summary, the highlights are as follows:

- The low-rank quaternion matrix completion via weighted Schatten p-norm minimization under the learnable transforms is suggested for color image recovery, which provides a satisfactory trade-off between efficiency and quality, especially for large-scale data.
- We develop an efficient alternating direction method of multipliers (ADMM) algorithm to address the resulting model and provide a weak convergence guarantee for the proposed algorithm, which is also validated by the numerical results. Experimental results on color images verify that the proposed method is considerably faster than state-of-art approaches while maintaining accuracy.

2. Notations and preliminaries

2.1. Notations

In this paper, $\mathbb{R}$, $\mathbb{C}$, and $\mathbb{Q}$ respectively denote the real space, complex space, and quaternion space. A scalar, a vector, and a matrix are written as x, $\mathbf{x}$, and $\mathbf{X}$, respectively. For quaternion algebra, a dot above the variables (e.g., $\dot{x}$, $\dot{\mathbf{x}}$, and $\dot{\mathbf{X}}$) is used to denote quaternion variables, and $\mathfrak{R}(\cdot)$ denotes the real part of quaternion variables.

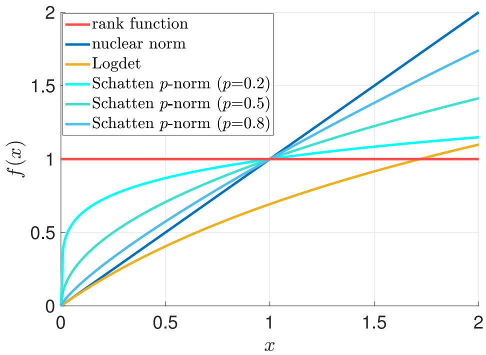

Fig. 1. One dimensional illustrations referring to different rank surrogates. x denotes the singular value, and $f(x)$ is the objective value.

2.2. Preliminaries

Preliminaries of quaternions (including quaternion numbers and quaternion matrices) can be seen in supplementary material (See Appendix A).

3. Proposed model and solving algorithm

3.1. Proposed model

The existing QNN-based matrix completion methods involve the QSVD based low-rank approximation, which suffers from high computational cost when dealing with large-scale tensor data. To overcome this issue, we introduce the data-driven semi-orthogonal transforms to project the large-scale quaternion matrix onto the small-scale quaternion matrix. For a target quaternion matrix $\dot{\mathbf{X}}$, the learnable semi-orthogonal transforms can be formulated as follows:

$$\dot{\mathbf{X}} = \dot{\mathbf{D}}_1^H \dot{\mathbf{Z}} \dot{\mathbf{D}}_2, \tag{2}$$

where $\dot{\mathbf{X}} \in \mathbb{Q}^{I_1 \times I_2}$ is the large-scale target quaternion matrix, $\dot{\mathbf{Z}} \in \mathbb{Q}^{r_1 \times r_2}$ is the small-scale essential quaternion matrix, and $\dot{\mathbf{D}}_i \in \mathbb{Q}^{r_i \times I_i} (i = 1, 2)$ are the semi-orthogonal transforms satisfying $\dot{\mathbf{D}}_i \dot{\mathbf{D}}_i^H = \mathbf{I} \in \mathbb{R}^{r_i \times r_i}$. Here, the semi-orthogonal transforms $\dot{\mathbf{D}}_i \dot{\mathbf{D}}_i^H = \mathbf{I}$ are crucial. Under this transform, the size of the transformed quaternion matrix $\dot{\mathbf{Z}}$ is smaller than the target quaternion matrix $\dot{\mathbf{X}}$, enjoying cheaper computational cost.

Non-convex relaxation techniques for accurate approximation of the rank function have shown promising performance in matrix completion or similar models [14,18,19]. Inspired by this, we pick out the weighted Schatten p-norm as the nonconvex surrogate of the quaternion rank to depict the low-rankness of $\dot{\mathbf{Z}}$ more accurately and efficiently. The weighted Schatten p-norm of $\dot{\mathbf{Z}}$ is defined as $\|\dot{\mathbf{Z}}\|_{w,S_p} = \sum_{i=1}^{\min\{r_1,r_2\}} w\sigma_i^p(\dot{\mathbf{Z}})$, where $w > 0$, $0 < p < 1$, and σ_i $(i = 1, 2, \ldots, \min\{r_1, r_2\})$ is the ith singular value of $\dot{\mathbf{Z}}$. The reason for taking the non-convex weighted Schatten p-norm into LRQMC is that it approximates the rank($\dot{\mathbf{Z}}$) more precisely than the nuclear norm (see Fig. 1).

Therefore, based on the proposed semi-orthogonal transforms and quaternion-based weighted Schatten p-norm, the following TN-LRQMC model for color image recovery is suggested:

$$\min_{\dot{\mathbf{Z}},\dot{\mathbf{X}},\dot{\mathbf{D}}_i} \quad \|\dot{\mathbf{Z}}\|_{w,S_p} \ \text{ s.t. } \dot{\mathbf{X}} = \dot{\mathbf{D}}_1^H \dot{\mathbf{Z}} \dot{\mathbf{D}}_2, \quad \dot{\mathbf{D}}_i \dot{\mathbf{D}}_i^H = \mathbf{I}_{r_i \times r_i}, \quad P_\Omega(\dot{\mathbf{X}}) = P_\Omega(\dot{\mathbf{Y}}). \tag{3}$$

3.2. Solving algorithm for the proposed model

To solve the proposed model, we first introduce the indicator function $\Psi(\dot{\mathbf{D}}_i) = \begin{cases} 0, & \dot{\mathbf{D}}_i\dot{\mathbf{D}}_i^H = \mathbf{I}_{r_i\times r_i}, \\ \infty, & \text{otherwise.} \end{cases}$ Then, the problem (3) can be rewritten as

$$\min_{\dot{\mathbf{Z}},\dot{\mathbf{X}},\dot{\mathbf{D}}_i} \|\dot{\mathbf{Z}}\|_{w,S_p} + \sum_{i=1}^{2} \Psi(\dot{\mathbf{D}}_i) \qquad \text{s.t. } \dot{\mathbf{X}} = \dot{\mathbf{D}}_1^H\dot{\mathbf{Z}}\dot{\mathbf{D}}_2, P_\Omega(\dot{\mathbf{X}}) = P_\Omega(\dot{\mathbf{Y}}). \tag{4}$$

We design an ADMM-based algorithm to solve the model (4). By introducing the Lagrangian multiplier $\dot{\mathbf{\Lambda}} \in \mathbb{Q}^{I_1\times I_2}$, the augmented Lagrangian function of (4) is given by

$$\begin{aligned} f(\dot{\mathbf{Z}},\dot{\mathbf{X}},\dot{\mathbf{D}}_i,\dot{\mathbf{\Lambda}}) =& \|\dot{\mathbf{Z}}\|_{w,S_p} + \sum_{i=1}^{2} \Psi(\dot{\mathbf{D}}_i) + \frac{\beta}{2}\|\dot{\mathbf{X}} - \dot{\mathbf{D}}_1^H\dot{\mathbf{Z}}\dot{\mathbf{D}}_2\|_F^2 \\ &+ \Re\left\langle \dot{\mathbf{X}} - \dot{\mathbf{D}}_1^H\dot{\mathbf{Z}}\dot{\mathbf{D}}_2, \dot{\mathbf{\Lambda}}\right\rangle + \frac{1}{2}\|P_\Omega(\dot{\mathbf{X}} - \dot{\mathbf{Y}})\|_F^2, \end{aligned} \tag{5}$$

where β is the penalty parameter. Within the scheme of the ADMM, we can update these variables in Eq. (5) by solving the following iterative subproblems.

1) *Update* $\dot{\mathbf{Z}}$. $\dot{\mathbf{Z}}$ subproblem is

$$\dot{\mathbf{Z}}^{t+1} = \arg\min_{\dot{\mathbf{Z}}} \|\dot{\mathbf{Z}}\|_{w,S_p} + \frac{\beta^t}{2}\|\dot{\mathbf{X}}^t - (\dot{\mathbf{D}}_1^t)^H\dot{\mathbf{Z}}\dot{\mathbf{D}}_2^t + \frac{\dot{\mathbf{\Lambda}}^t}{\beta^t}\|_F^2. \tag{6}$$

To solve the above problem, we introduce the following lemma.

Lemma 1. *Let $\dot{\mathbf{D}}_1 \in \mathbb{Q}^{r_1\times I_1}$ and $\dot{\mathbf{D}}_2 \in \mathbb{Q}^{r_2\times I_2}$ be the semi-orthogonal quaternion matrix, i.e., $\dot{\mathbf{D}}_i\dot{\mathbf{D}}_i^H = \mathbf{I}_{r_i\times r_i}(i=1,2)$, where $\mathbf{I}$ is the identity matrix. Then we have*

$$\arg\min_{\dot{\mathbf{Z}}} \|\dot{\mathbf{X}} - \dot{\mathbf{D}}_1^H\dot{\mathbf{Z}}\dot{\mathbf{D}}_2\|_F^2 = \arg\min_{\dot{\mathbf{Z}}} \|\dot{\mathbf{D}}_1\dot{\mathbf{X}}\dot{\mathbf{D}}_2^H - \dot{\mathbf{Z}}\|_F^2, \tag{7}$$

where $\dot{\mathbf{X}} \in \mathbb{Q}^{I_1\times I_2}$ and $\dot{\mathbf{Z}} \in \mathbb{Q}^{r_1\times r_2}$.

The proof of Lemma 1 can be found in supplementary material (See Appendix B). Using Lemma 1, $\dot{\mathbf{Z}}$ subproblem can be equivalently formulated as follows:

$$\dot{\mathbf{Z}}^{t+1} = \arg\min_{\dot{\mathbf{Z}}} \|\dot{\mathbf{Z}}\|_{w,S_p} + \frac{\beta^t}{2}\|\dot{\mathbf{D}}_1^t\left(\dot{\mathbf{X}}^t + \dot{\mathbf{\Lambda}}^t/\beta^t\right)(\dot{\mathbf{D}}_2^t)^H - \dot{\mathbf{Z}}\|_F^2. \tag{8}$$

According to Theorem 3 in [14], (8) can be solved by

$$\dot{\mathbf{Z}}^{t+1} = \dot{\mathbf{U}}\mathbf{\Sigma}^{\nabla\phi/\beta^t}\dot{\mathbf{V}}^H, \tag{9}$$

where $\dot{\mathbf{U}}\mathbf{\Sigma}\dot{\mathbf{V}}^H$ is the QSVD of $\dot{\mathbf{D}}_1^t\left(\dot{\mathbf{X}}^t + \dot{\mathbf{\Lambda}}^t/\beta^t\right)(\dot{\mathbf{D}}_2^t)^H \in \mathbb{Q}^{r_1\times r_2}$, $\mathbf{\Sigma}^{\nabla\phi/\beta^t} = \max\{\mathbf{\Sigma} - \nabla\phi(\sigma^t)/\beta^t, 0\}$, $\nabla\phi(\sigma^t) = wp(\sigma^t)^{p-1}$ is the gradient of weighted Schatten p-norm at σ^t, and σ^t is the singular value of $\dot{\mathbf{Z}}$ at the tth (previous) iteration.

2) *Update* $\dot{\mathbf{X}}$. $\dot{\mathbf{X}}$ subproblem is

$$\dot{\mathbf{X}}^{t+1} = \arg\min_{\dot{\mathbf{X}}} \frac{\beta^t}{2}\|\dot{\mathbf{X}} - (\dot{\mathbf{D}}_1^t)^H\dot{\mathbf{Z}}^{t+1}\dot{\mathbf{D}}_2^t + \frac{\dot{\mathbf{\Lambda}}^t}{\beta^t}\|_F^2 + \frac{1}{2}\|P_\Omega(\dot{\mathbf{X}} - \dot{\mathbf{Y}})\|_F^2, \tag{10}$$

which has the following closed-form solution

$$\dot{\mathbf{X}}^{t+1} = P_{\Omega^c}\left((\dot{\mathbf{D}}_1^t)^H\dot{\mathbf{Z}}^{t+1}\dot{\mathbf{D}}_2^t - \dot{\mathbf{\Lambda}}^t/\beta^t\right) + P_{\Omega}\left((\beta^t(\dot{\mathbf{D}}_1^t)^H\dot{\mathbf{Z}}^{t+1}\dot{\mathbf{D}}_2^t - \dot{\mathbf{\Lambda}}^t + \dot{\mathbf{Y}})/(1+\beta^t)\right), \tag{11}$$

where Ω^c denotes the complementary set of Ω.

3) *Update* $\dot{\mathbf{D}}_i\{i=1,2\}$. For $\dot{\mathbf{D}}_1$ subproblem, we have

$$\dot{\mathbf{D}}_1^{t+1} = \arg\min_{\dot{\mathbf{D}}_1} \frac{\beta^t}{2}\|\dot{\mathbf{X}}^{t+1} - \dot{\mathbf{D}}_1^H\dot{\mathbf{Z}}^{t+1}\dot{\mathbf{D}}_2^t + \frac{\dot{\mathbf{\Lambda}}^t}{\beta^t}\|_F^2 + \Psi(\dot{\mathbf{D}}_1). \tag{12}$$

Note that the problem (12) can be equivalently transformed into the following problem:

$$\begin{aligned} &\arg\min_{\dot{\mathbf{D}}_1} \frac{\beta^t}{2}\|(\dot{\mathbf{X}}^{t+1} + \frac{\dot{\mathbf{\Lambda}}^t}{\beta^t})(\dot{\mathbf{D}}_2^t)^H - \dot{\mathbf{D}}_1^H\dot{\mathbf{Z}}^{t+1}\|_F^2 + \Psi(\dot{\mathbf{D}}_1) \\ &= \arg\max_{\dot{\mathbf{D}}_1} \Re(\mathrm{Tr}(\beta^t\dot{\mathbf{A}}^{t+1}(\dot{\mathbf{Z}}^{t+1})^H\dot{\mathbf{D}}_1)) - \Psi(\dot{\mathbf{D}}_1), \end{aligned} \tag{13}$$

where $\dot{\mathbf{A}}^{t+1} = (\dot{\mathbf{X}}^{t+1} + \frac{\dot{\mathbf{\Lambda}}^t}{\beta^t})(\dot{\mathbf{D}}_2^t)^H$. Supposing the QSVD of $\beta\dot{\mathbf{A}}^{t+1}(\dot{\mathbf{Z}}^{t+1})^H$ is $\dot{\mathbf{U}}\mathbf{S}\dot{\mathbf{V}}^H$, we have $\Re(\mathrm{Tr}(\dot{\mathbf{U}}\mathbf{S}\dot{\mathbf{V}}^H\dot{\mathbf{D}}_1)) = \Re(\mathrm{Tr}(\mathbf{S}\dot{\mathbf{V}}^H\dot{\mathbf{D}}_1\dot{\mathbf{U}}))$. Since $\mathbf{S}$ is the diagonal matrix, the problem (13) can be maximized when the diagonal elements of $\dot{\mathbf{V}}^H\dot{\mathbf{D}}_1\dot{\mathbf{U}}$ are positive and maximum. Under the orthogonal procrustes problem [20], this is achieved when $\dot{\mathbf{D}}_1 = \dot{\mathbf{V}}\dot{\mathbf{U}}(:,1:r_1)^H$ in which case the diagonal elements are all 1. Thus, the closed-form solution of (12) is

$$\dot{\mathbf{D}}_1^{t+1} = \dot{\mathbf{V}}\dot{\mathbf{U}}(:,1:r_1)^H. \tag{14}$$

Similarly, the solution of $\dot{\mathbf{D}}_2$ subproblem is

$$\dot{\mathbf{D}}_2^{t+1} = \dot{\mathbf{N}}\dot{\mathbf{M}}(:,1:r_1)^H, \tag{15}$$

where $\dot{\mathbf{M}}\mathbf{\Sigma}\dot{\mathbf{N}}^H$ is the QSVD of $\beta^t(\dot{\mathbf{X}}^{t+1} + \frac{\dot{\mathbf{\Lambda}}^t}{\beta^t})^H(\dot{\mathbf{D}}_1^{t+1})^H\dot{\mathbf{Z}}^{t+1}$.

We summarize the ADMM for the proposed method in Algorithm 1.

Algorithm 1 The ADMM algorithm for solving (3)

Input: The incomplete quaternion matrix $\dot{\mathbf{Y}} \in \mathbb{Q}^{I_1\times I_2}$, Ω, $r_i(i=1,2)$, β^0, $\beta^{\max}$, and $\rho = 1.1$.
1: **Initialize:** $\dot{\mathbf{X}}^0 = \dot{\mathbf{Y}}$, $[\dot{\mathbf{U}}_1,\mathbf{S}_1,\dot{\mathbf{V}}_1] = \mathrm{QSVD}(\dot{\mathbf{X}}^0)$, $\dot{\mathbf{D}}_1^0 = \dot{\mathbf{U}}_1(:,1:r)^H$, $[\dot{\mathbf{U}}_2,\mathbf{S}_2,\dot{\mathbf{V}}_2] = \mathrm{QSVD}((\dot{\mathbf{X}}^0)^H)$, $\dot{\mathbf{D}}_2^0 = \dot{\mathbf{U}}_2(:,1:r)^H$.
2: **while** not converged and $t < 500$ **do**
3: Update $\dot{\mathbf{Z}}^{t+1}$ via (9).
4: Update $\dot{\mathbf{X}}^{t+1}$ via (11).
5: Update $\dot{\mathbf{D}}_1^{t+1}$ and $\dot{\mathbf{D}}_2^{t+1}$ via (14) and (15).
6: Update $\dot{\Lambda}^{t+1}$ via $\dot{\Lambda}^{t+1} = \dot{\Lambda}^t + \beta^t(\dot{\mathbf{X}}^{t+1} - (\dot{\mathbf{D}}_1^{t+1})^H\dot{\mathbf{Z}}^{t+1}\dot{\mathbf{D}}_2^{t+1})$.
7: Update β^{t+1} via $\beta^{t+1} = \min(\rho\beta^t, \beta^{\max})$.
8: Check the convergence condition: $\|\dot{\mathbf{X}}^{t+1} - \dot{\mathbf{X}}^t\|_F/\|\dot{\mathbf{X}}^t\|_F \le 10^{-4}$.
9: **end while**
Output: The recovered quaternion matrix $\dot{\mathbf{X}}$.

3.3. Computational complexity

In this part, we discuss the computational complexity of the proposed TN-LRQMC model. As shown in Algorithm 1, for the input quaternion matrix $\dot{\mathbf{X}} \in \mathbb{R}^{I_1\times I_2}$, the computational complexity at each iteration of the developed algorithm can be concluded by updating $\dot{\mathbf{Z}}$, updating $\dot{\mathbf{X}}$, updating $\dot{\mathbf{D}}_1$, and updating $\dot{\mathbf{D}}_2$, which cost $O(I_1I_2r_1 + I_2r_1r_2 + 2\min(r_1^2r_2, r_1r_2^2))$, $O(I_1r_1r_2 + I_1I_2r_2)$, $O(I_1I_2r_2 + I_1r_1r_2 + I_1r_1^2 + I_1^2r_1)$, and $O(I_1I_2r_1 + I_2r_1r_2 + I_2r_2^2 + I_2^2r_2)$, respectively. Thus, the total cost at each iteration of the developed algorithm is $O(I_1^2r_1 + I_2^2r_2 + 2I_1I_2(r_1+r_2) + 2r_1r_2(I_1+I_2))$.

3.4. Convergence analysis

Here, we prove the weak convergence of Algorithm 2 in Theorem 2, which is essential to guarantee that the iterative sequence can attain a stable solution.

Theorem 2 (*Convergence*)**.** *Let $\{\dot{\mathbf{Z}}^t, \dot{\mathbf{X}}^t, \dot{\mathbf{D}}_i^t, \dot{\mathbf{\Lambda}}^t\}_{t=1}^{\infty}$ be the sequences generated by Algorithm 1, assuming $\dot{\mathbf{\Lambda}}^{t+1} - \dot{\mathbf{\Lambda}}^t \to 0$, and $\{\dot{\mathbf{\Lambda}}^t\}$ is bounded. Then*

(a) The sequence $\{\dot{\mathbf{Z}}^t, \dot{\mathbf{X}}^t, \dot{\mathbf{D}}_i^t\}_{t=1}^{\infty}$ is bounded;

(b) The sequence $\{\dot{\mathbf{X}}^t, (\dot{\mathbf{D}}_1^t)^H \dot{\mathbf{Z}}^t \dot{\mathbf{D}}_2^t\}_{t=1}^{\infty}$ is Cauchy sequence;

(c) Any accumulation point of $\{\dot{\mathbf{Z}}^t, \dot{\mathbf{X}}^t, \dot{\mathbf{D}}_i^t, \dot{\mathbf{\Lambda}}^t\}_{t=1}^{\infty}$ is a stationary Karush-Kuhn–Tucker point of Eq. (5).

The proof of Theorem 2 can be found in supplementary material (See Appendix B).

4. Numerical experiments

This section conducts color images recovery experiments on Berkeley Segmentation Dataset[1] and Kodak PhotoCD Dataset[2] to demonstrate the superiority and effectiveness of our TN-LRQMC method. The compared approaches are LRQA-1 [14], LRQA-4 [14], QLNF [17], and TQLNA [17]. In all experiments, parameters corresponding to compared methods are carefully adjusted according to the reference papers' suggestions. The peak signal-to-noise ratio (PSNR) and structural similarity index (SSIM) [21] are adopted to evaluate the recovered results. Larger PSNR and SSIM indicate the result is better. In all experiments, incomplete data are generated by sampling elements of images randomly for different sample ratios (SRs) from $\{0.1, 0.2, 0.3\}$.

4.1. Experimental results

Table 1 reports the quantitative results of competitive methods on test images with different SRs. The best and second best values are, respectively, highlighted in boldface and underlined. The PSNR results are also shown for a more clear visual comparison (See Appendix C, available in supplementary material). The following conclusions can be drawn from the above experimental results. (1) The recovered results by TN-LRQMC are quantitatively (see Table 1) and visually close to the recovered results by LRQA-4 and TQLNA. (2) Note that in terms of computation time among all methods, the proposed TN-LRQMC is the fastest on the test data sets (see Table 1). Particularly, when the size of the color image is $512 \times 768 \times 3$, it is nearly seven times faster than TQLNA, and at least nine times faster than LRQA-4. The reason is that our method projects the large-scale target quaternion matrix into the small-scale quaternion matrix, reducing the computation burden of large quaternion matrices. In summary, TN-LRQMC achieves substantial speedup while maintaining accuracy compared with other methods.

4.2. Numerical convergence

In this subsection, we show the numerical convergence of the proposed algorithm. In Fig. 2, we display the relative error ($\|\dot{\mathbf{X}}^{t+1} - \dot{\mathbf{X}}^t\|_F / \|\dot{\mathbf{X}}^t\|_F$) curves of the ADMM algorithm (in the logarithmic scale) with respect to iterations on all color images. We observe that although there have fluctuations at the beginning of the convergence curves, the overall trend is decreasing steadily, which demonstrates the numerical stability and the convergence of the proposed method.

[1] https://www2.eecs.berkeley.edu/Research/Projects/CS/vision/bsds/
[2] http://r0k.us/graphics/kodak/

Table 1
PSNR, SSIM, and running time (in second) of results by different methods with different SRs on color images.

Data	Method	SR = 0.1			SR = 0.2			SR = 0.3		
		PSNR	SSIM	Time	PSNR	SSIM	Time	PSNR	SSIM	Time
	Observed	7.41	0.039	–	7.92	0.091	–	8.50	0.154	–
	LRQA-1	17.13	**0.735**	381	19.93	0.820	373	21.98	0.872	393
	LRQA-4	**18.05**	0.730	881	**20.90**	**0.822**	1051	22.95	**0.876**	1168
	QLNF	17.70	0.705	1779	20.45	0.802	1888	22.23	0.854	1808
	TQLNA	17.85	0.721	771	20.72	0.809	832	**22.97**	0.868	768
Image01 321 × 481 × 3	TN-LRQMC	17.97	0.726	**219**	20.88	0.819	**227**	22.93	0.872	**242**
	Observed	10.14	0.077	–	10.64	0.143	–	11.23	0.219	–
	LRQA-1	18.57	0.601	397	21.41	0.727	382	23.49	0.810	368
	LRQA-4	19.58	0.610	921	**22.52**	**0.743**	962	24.85	**0.831**	981
	QLNF	19.33	0.594	1139	21.99	0.716	1695	23.78	0.789	1536
	TQLNA	19.31	0.589	782	22.42	0.735	776	**24.92**	0.830	715
Image02 321 × 481 × 3	TN-LRQMC	**19.62**	**0.613**	**226**	**22.52**	0.742	**221**	24.86	0.829	**221**
	Observed	9.17	0.038	–	9.68	0.103	–	10.26	0.184	–
	LRQA-1	24.56	0.954	1272	26.66	0.967	1169	28.11	0.975	1126
	LRQA-4	25.16	**0.955**	4518	27.32	**0.969**	4797	28.73	0.977	4797
	QLNF	24.00	0.943	2960	26.38	0.962	3214	27.94	0.972	3269
	TQLNA	25.05	0.952	3316	**27.34**	0.968	3256	**28.98**	**0.978**	4849
Image03 512 × 768 × 3	TN-LRQMC	**25.20**	0.954	**485**	27.24	**0.969**	**485**	28.55	0.976	**486**
	Observed	8.00	0.024	–	8.50	0.051	–	9.09	0.081	–
	LRQA-1	22.63	0.773	1377	25.46	0.865	1398	27.24	0.904	1352
	LRQA-4	23.67	**0.794**	4395	26.48	**0.870**	4366	28.15	**0.908**	4511
	QLNF	23.61	0.764	2527	25.90	0.850	1956	27.19	0.886	1692
	TQLNA	23.57	0.763	3499	**26.54**	0.852	3329	**28.48**	0.897	3002
Image04 512 × 768 × 3	TN-LRQMC	**23.99**	0.793	**442**	26.41	0.865	**467**	27.98	0.900	**489**

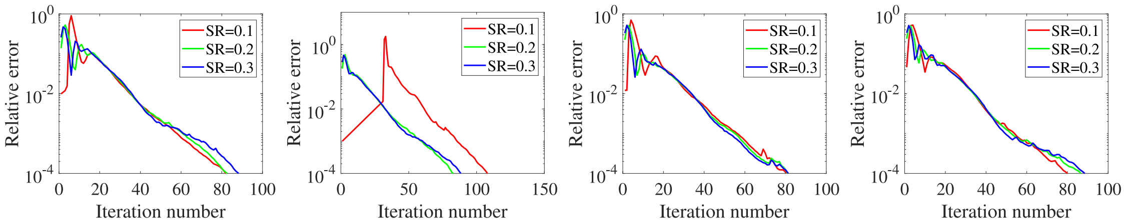

(a) image01 (b) image02 (c) image03 (d) image04

Fig. 2. Curves of relative errors versus iterations on all images with different SRs.

5. Conclusion

In this letter, we proposed a low-rank quaternion matrix completion via nonconvex function approximation under the learnable transforms for color image recovery. More specifically, we first projected the large-scale quaternion matrix to the small-scale quaternion matrix by the learnable semi-orthogonal transforms along each mode. Then, we adopted the weighted Schatten p-norm to achieve a more precise rank estimation of the small-scale quaternion matrix. The alternating direction method of multipliers algorithm with convergence guarantee is given to solve the proposed model. Experimental results on color images demonstrate that the proposed method achieved a satisfactory trade-off between efficiency and quality for large-scale quaternion matrix processing.

Data availability

Data will be made available on request.

Acknowledgments

This research is supported by University of Macau (MYRG2022-00108-FST, MYRG-CRG2022-00010-ICMS), The Science and Technology Development Fund, Macau S.A.R (0036/2021/AGJ) and Chinese Guangdong's S&T project (2022A0505020028).

Appendix A. Supplementary data

Supplementary material related to this article can be found online at https://doi.org/10.1016/j.aml.2023.108880.

References

[1] T. Zhang, J. Zhao, Q. Sun, B. Zhang, J. Chen, M. Gong, Low-rank tensor completion via combined tucker and tensor train for color image recovery, Appl. Intell. (2022) 1–16.
[2] F. Nie, Z. Hu, X. Li, Matrix completion based on non-convex low-rank approximation, IEEE Trans. Image Process. 28 (5) (2019) 2378–2388.
[3] M. Zheng, G. Ni, Approximation strategy based on the T-product for third-order quaternion tensors with application to color video compression, Appl. Math. Lett. 140 (2023) 108587.
[4] Z. Jia, K. NG, G. Song, Robust quaternion matrix completion with applications to image inpainting, Numer. Linear Algebra Appl. 26 (4) (2019).
[5] F. Zhang, Quaternions and matrices of quaternions, Linear Algebra Appl. 251 (1997) 21–57.
[6] Z. Qin, Z. Ming, L. Zhang, Singular value decomposition of third order quaternion tensors, Appl. Math. Lett. 123 (2022) 107597.
[7] C. Huang, M.K. Ng, T. Wu, T. Zeng, Quaternion-based dictionary learning and saturation-value total variation regularization for color image restoration, IEEE Trans. Multimed. 24 (2022) 3769–3781.
[8] Z. Jia, Q. Jin, M.K. Ng, X. Zhao, Non-local robust quaternion matrix completion for large-scale color image and video inpainting, IEEE Trans. Image Process. 31 (2022) 3868–3883.
[9] C. Huang, Z. Li, Y. Liu, T. Wu, T. Zeng, Quaternion-based weighted nuclear norm minimization for color image restoration, Pattern Recognit. 128 (2022) 108665.
[10] Q. Yin, J. Wang, X. Luo, J. Zhai, S.K. Jha, Y. Shi, Quaternion convolutional neural network for color image classification and forensics, IEEE Access 7 (2019) 20293–20301.
[11] R. Lan, Y. Zhou, Quaternion-michelson descriptor for color image classification, IEEE Trans. Image Process. 25 (11) (2016) 5281–5292.
[12] Y. Sun, S. Chen, B. Yin, Color face recognition based on quaternion matrix representation, Pattern Recognit. Lett. 32 (4) (2011) 597–605.
[13] C. Zou, K.I. Kou, Y. Wang, Quaternion collaborative and sparse representation with application to color face recognition, IEEE Trans. Image Process. 25 (7) (2016) 3287–3302.
[14] Y. Chen, X. Xiao, Y. Zhou, Low-rank quaternion approximation for color image processing, IEEE Trans. Image Process. 29 (2020) 1426–1439.
[15] J. Miao, K.I. Kou, Quaternion-based bilinear factor matrix norm minimization for color image inpainting, IEEE Trans. Signal Process. 68 (2020) 5617–5631.
[16] L. Yang, K.I. Kou, J. Miao, Weighted truncated nuclear norm regularization for low-rank quaternion matrix completion, J. Vis. Commun. Image Represent. 81 (2021) 103335.
[17] L. Yang, J. Miao, K.I. Kou, Quaternion-based color image completion via logarithmic approximation, Inform. Sci. 588 (2022) 82–105.
[18] C. Lu, J. Tang, S. Yan, Z. Lin, Nonconvex nonsmooth low rank minimization via iteratively reweighted nuclear norm, IEEE Trans. Image Process. 25 (2) (2016) 829–839.
[19] J. Xu, Y. Cheng, Y. Ma, Weighted schatten p-norm low rank error constraint for image denoising, Entropy 23 (2) (2021) 158.
[20] P.H. Schönemann, A generalized solution of the orthogonal procrustes problem, Psychometrika 31 (1) (1966) 1–10.
[21] Z. Wang, A. Bovik, H. Sheikh, E. Simoncelli, Image quality assessment: from error visibility to structural similarity, IEEE Trans. Image Process. 13 (4) (2004) 600–612.